Lattice Boltzmann Simulation for Complex Flow in a Solar Wall*

CHEN Rou (陈柔),[1,2] Shao Jiu-Gu (邵九姑),[1] ZHENG You-Qu (郑友取),[3] YU Hui-Dan (俞慧丹),[2,4] and XU You-Sheng (许友生)[1,3,†]

[1]Department of Physics, Zhejiang Normal University, Jinhua 321004, China

[2]Department of Mechanical Engineering, Indiana University-Purdue University Indianapolis, Indianapolis, IN 46202, USA

[3]School of Light Industry, Zhejiang University of Science and Technology, Hangzhou 310023, China

[4]College of Metrology & Measurement Engineering, Zhongguo Jiliang University, Hangzhou 310018, China

(Received October 18, 2012; revised manuscript received December 13, 2012)

Abstract *In this letter, we present a lattice Boltzmann simulation for complex flow in a solar wall system which includes porous media flow and heat transfer, specifically for solar energy utilization through an unglazed transpired solar air collector (UTC). Besides the lattice Boltzmann equation (LBE) for time evolution of particle distribution function for fluid field, we introduce an analogy, LBE for time evolution of distribution function for temperature. Both temperature fields of fluid (air) and solid (porous media) are modeled. We study the effects of fan velocity, solar radiation intensity, porosity, etc. on the thermal performance of the UTC. In general, our simulation results are in good agreement with what in literature. With the current system setting, both fan velocity and solar radiation intensity have significant effect on the thermal performance of the UTC. However, it is shown that the porosity has negligible effect on the heat collector indicating the current system setting might not be realistic. Further examinations of thermal performance in different UTC systems are ongoing. The results are expected to present in near future.*

PACS numbers: 47.56.+r, 44.30.+v, 47.11.Qr
Key words: solar wall system, complex flow, lattice Boltmann similation

Kinetic-based lattice Boltzmann method (LBM) has been developed rapidly in the last two decades and becomes a powerful numerical simulation tool for computing various complex flows.[1−2] The method is second-order accurate in time and space and recovers Navier–Stokes equations in the incompressible limit.[3] The main physical and computational advantages of LBM include simplicity of programming, ease of handling complex geometry, suitability of massive parallel computing, etc. thus it is well suited for simulating complex flows including multiprocess multi-physics, for instances, magnetofluids,[4] chemical reaction flow,[5] multiphase and multicomponent flow,[6−9] porous flow,[10−11] and non-Newtonian fluids.[12]

Due to the high ventilation rates in commercial and industrial buildings, heating should be very expensive. As a result, installing a "solar wall" to heat air before it enters a building, has become one of the most efficient ways of reducing energy costs using clean and renewable energy.[13] Solar wall systems provide solar-heated fresh air to the buildings and have a higher efficiency than traditional glass solar collectors.[14] There have been efforts to study the thermal performance of a solar wall experimentally and numerically for the purpose to develop this elegant technology. Based on the overall performance of the solar collector, Kutscher *et al.*[15] presented a computational fluid dynamic (CFD) model to show that both the heating and airflow should be uniform in order to achieve a high heat transfer rate. Later, the same group developed a pipe network method[16] to analyze the airflow distribution incorporating their previous research results for the heat exchange effectiveness, pressure drop, and wind heat loss, but the accuracy of the model was low for a short pipe system. Thus it was used instead of the cavity in a negative pressure zone of a real system. Heat transfer through the pores of a heat collector has been simulated using a computational fluid dynamics (CFD) model[17] discussing five parameters that affected the heat exchange effectiveness under no-wind conditions. Hollick[18−20] systematically studied the performance for wind directions parallel to the solar collector. Wang and Liu[21] found experimentally that the porosity of the solar wall combination has a large influence on the heat effect.

In this paper, we develop LBM to simulate complex flow in a solar wall system which includes porous media flow and heat transfer. Focus is on factors that affect thermal performance in the system. The solar wall system we simulate is an unglazed transpired solar air collector (UTC) shown in Fig. 1. It is a passive solar heating system in which the absorption surface with a selective coating faces south and converts solar energy into heat. The coating is a material with a high heat absorptivity. It has been known that UTCs typically have a high heat ef-

*Supported by the National Nature Science Foundation of China under Grant Nos. 10932010, 11072220, 11072229, U1262109, 51176172, and 10972208

†Corresponding author, E-mail: whyu@iupui.edu; ysyou@zjnu.cn

ficiency, provide a well-designed fresh air system,[22] yield good economic returns, and have a wide range of applications and energy saving benefits.[23] The UTC consists of the absorption surface and a porous solar wall. A canopy covers the external wall of the building, a gap between the porous solar wall and building wall, and an exhaust fan to extract the air in the gap and feed it into the ducting system. The function of a UTC is twofold. In winter, cool fresh air absorbs heat from the heated coating faces and porous media during daytime and enters the ventilation system to heat the building. At night, the heat lost through the wall is absorbed by the flowing air in the cavity and re-enters the room when the fan is on. In this way, both fresh air and also heated air are supplied by using the wall as a heat exchanger. In summer, the fans are switched off so that hot air passes straight through the lower and upper gaps of the solar wall without entering the room.[24−26] In this work, we focus on the heating function in winter to study the thermal performance.

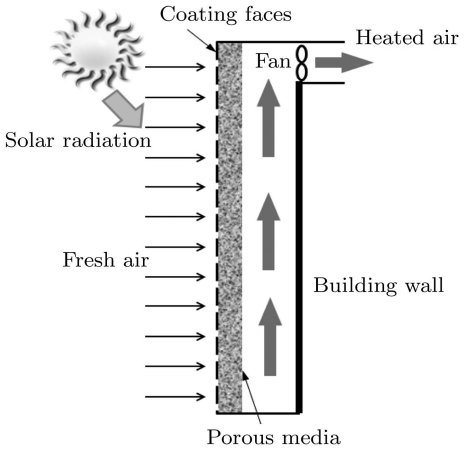

Fig. 1 Schematic of the unglazed transpired solar air collector.

Assuming that the Boussinesq limit holds, the governing equations of the fluid dynamics and heat transfer in the solar wall system can be described as follows:

$$\nabla \cdot \boldsymbol{u} = 0\,, \tag{1}$$

$$\frac{\partial \boldsymbol{u}}{\partial t} + (\boldsymbol{u}\cdot\nabla)\frac{\boldsymbol{u}}{\phi} = \frac{1}{\rho_f}\nabla\phi P + \nabla\cdot(\upsilon_\varepsilon\nabla\boldsymbol{u}) + \boldsymbol{F}\,, \tag{2}$$

$$\sigma\frac{\partial T_f}{\partial t} + \boldsymbol{u}\cdot\nabla T_f = \nabla(\alpha_{f\varepsilon}\nabla T_f) + S_f\,, \tag{3}$$

$$\sigma\frac{\partial T_s}{\partial t} = \nabla(\alpha_{s\varepsilon}\nabla T_s) + S_s\,. \tag{4}$$

The notations appeared in Eq. (2) to Eq. (4) are explained as follows.

- Symbol ϕ is the porosity of the porous medium, υ_ε is the effective viscosity, α_s and α_f are the thermal diffusivities of the solid and gas phases respectively, and h_υ is the volumetric heat transfer coefficient between the fluid and the porous media skeleton. Both α_s and α_f are fixed for the calculations shown here. The ratio of the heat capacities of the pure substance C_{ps} and porous medium C_{pf} is given by $\sigma = \phi + (1-\phi)\rho_s C_{ps}/\rho_f C_{pf}$, and here, σ is taken as unity.

- Terms S_f and S_s in Eqs. (3) and (4) are sources for fluid and solid phases respectively and defined as

$$S_f = h_\upsilon(T_s - T_f)\,, \tag{5}$$

$$S_s = -h_\upsilon(T_s - T_f)\,, \tag{6}$$

  where $\boldsymbol{u}$, P, T_f, and T_s are the volume-averaged velocity, pressure, temperature of the gas phase and that of the solid phase, respectively.

- The total force $\boldsymbol{F}$ can be described as

$$\boldsymbol{F} = \frac{\phi\upsilon}{K}\boldsymbol{u} - \frac{\phi F_\phi}{\sqrt{K}}|\boldsymbol{u}|\boldsymbol{u} + \phi\boldsymbol{G}\,, \tag{7}$$

  where the first term is the interaction force of the material and porous medium, the second term is the influence of the geometric construction, and the last term is the body force: $\boldsymbol{G} = -g\beta(T - T_0)$,

$$K = \frac{\phi^3 d^2}{150(1-\phi)^2}\,, \quad F_\phi = \frac{1.75}{\sqrt{150\phi^3}}\,,$$

  with $\boldsymbol{G}$, d, K, and F_ϕ the buoyancy force, average particle diameter, permeability, and geometric function, respectively.

The governing equations (1) to Eq. (3) can be normalized using the non-dimensional parameters of the viscosity ratio J, the Darcy number Da, the Prandtl number Pr, and the Rayleigh number Ra, which are defined as

$$J = \frac{\upsilon_\varepsilon}{\upsilon}, \quad \mathrm{Da} = \frac{K}{L^2}, \quad \mathrm{Pr} = \frac{\upsilon}{\alpha_\varepsilon}, \quad \mathrm{Ra} = \frac{g\beta\Delta T L^3}{\upsilon\alpha_\varepsilon}, \tag{8}$$

with L the characteristic length and ΔT the maximum temperature difference in the system.

The lattice Boltzmann equation (LBE) with a force to reflect porous effect is

$$f_i(\boldsymbol{x} + c\boldsymbol{e}_i\Delta t, t+\Delta t) - f_i(\boldsymbol{x}, t) = -\frac{1}{\tau}[f_i(\boldsymbol{x},t) - f_i^{\mathrm{eq}}(\boldsymbol{x},t)] + \Delta t F_i\,, \tag{9}$$

where $\boldsymbol{e}_i$ are the discrete velocity directions, and τ is the relaxation time. In the present work, we choose the D2Q9 model thus the discrete velocities are given by

$$\boldsymbol{e}_i = \begin{cases} 0, & i = 0\,, \\ \Big(\cos\dfrac{(i-1)\pi}{2}, \sin\dfrac{(i-1)\pi}{2}\Big) & i = 1{-}4\,, \\ \sqrt{2}\Big(\cos\dfrac{(2i-9)\pi}{2}, \sin\dfrac{(2i-9)\pi}{2}\Big), & i = 5{-}8\,, \end{cases} \tag{10}$$

and the equilibrium distribution function (EDF) f_i^{eq} is defined as

$$f_i^{\mathrm{eq}} = \rho\omega_i\Big[1 + 3(\boldsymbol{e}_i\cdot\boldsymbol{u}) + 4.5\frac{(\boldsymbol{e}_i\cdot\boldsymbol{u})^2}{\phi} - 1.5\frac{\boldsymbol{u}\boldsymbol{u}}{\phi}\Big]. \tag{11}$$

The force term $\boldsymbol{F}_i$ is formulated as[27]

$$\boldsymbol{F}_i^{\mathrm{eq}} = \rho\omega_i\Big(1 - \frac{1}{2\tau}\Big)\Big[\frac{\boldsymbol{e}_i\boldsymbol{F}}{c_s^2} + \frac{\boldsymbol{u}F:(\boldsymbol{e}_i\cdot\boldsymbol{e}_i - c_s^2\boldsymbol{I})}{\phi c_s^4}\Big], \tag{12}$$

with weights of $\omega_0 = 4/9$, $\omega_i = 1/9$ for $i = 1$–4, and $\omega_i = 1/36$ for $i = 5$–8. Thus, the macroscopic flow velocity and pressure are given by

$$\boldsymbol{u} = \frac{\boldsymbol{v}}{c_0 + \sqrt{c_0^2 + c_1|\boldsymbol{v}|}}, \quad \rho = \sum_i f_i \,, \tag{13}$$

where c_0, c_1, and $\boldsymbol{v}$ are given by

$$c_0 = \frac{1}{2}\Big(1 + \phi\frac{\Delta t \nu_\varepsilon}{2K}\Big), \quad c_1 = \phi\frac{\Delta t F_\phi}{2\sqrt{K}} \,,$$
$$\boldsymbol{v} = \sum_i \frac{\boldsymbol{e}_i}{\rho} + \frac{\Delta t}{2}\phi\boldsymbol{G} \,. \tag{14}$$

Through Chapman–Enskog expansion, the macroscopic equations corresponding to Eq. (9) are as follows

$$\frac{\partial \rho}{\partial t} + \nabla\cdot(\rho\boldsymbol{u}) = 0 \,, \tag{15}$$

$$\frac{\partial \rho\boldsymbol{u}}{\partial t} + \nabla\cdot\Big(\frac{\rho\boldsymbol{u}\boldsymbol{u}}{\phi}\Big) = -\nabla p + \nabla[\rho\upsilon_\varepsilon(\nabla\boldsymbol{u} + \boldsymbol{u}\nabla)] + \rho\boldsymbol{F} \,, \tag{16}$$

where $p = c_s^2\rho/\phi$ is the pressure, and the viscosity ν_ε is given by

$$\nu_\varepsilon = c_s^2\Delta t(\tau - 0.5) \,. \tag{17}$$

In the incompressible limit ($\rho_0 = \rho_1 =$ constant), Eqs. (15) and (16) recover the governing equations of Eqs. (1) and (2), respectively.[28]

For the heat transfer in porous solar wall, the presence of the fresh air flow will affect the temperature distribution of the porous media. Analogy to the flow field, we introduce temperature distribution functions for fluid (air) and solid (porous) and construct the LBEs for the temperature fields coupled through heat transfer. The LBE of fluid phase for (Eq. (3)) reads[29−30]

$$T_{fi}(\boldsymbol{x} + c\boldsymbol{e}_i\Delta t, t + \Delta t) - T_{fi}(\boldsymbol{x}, t)$$
$$= -\frac{1}{\tau'}[T_{fi}(\boldsymbol{x}, t) - T_i^{\rm eq}(\boldsymbol{x}, t)] + \Delta t\Big(1 - \frac{1}{2\tau'}\Big)\omega_i S_f \,, \tag{18}$$

where $T_{fi}^{\rm eq}$ is an EDF for temperature has the following format

$$T_{fi}^{\rm eq} = \omega_i\cdot T\Big(1 + \frac{e_i\cdot\boldsymbol{u}}{c_s^2}\Big) \,, \tag{19}$$

through the Chapman–Enskog multiscaling expansion technique, Eq. (3) can be recovered as

$$\sigma\frac{\partial\, T_f}{\partial t} + \boldsymbol{u}\cdot\nabla\, T_f = \nabla(\alpha_f\nabla\, T_f) + S_f \,. \tag{20}$$

The thermal conductivity is then given by

$$\alpha_{f\varepsilon} = \sigma c_s^2\Delta t(\tau' - 0.5) \,. \tag{21}$$

The temperature of the gas phase is defined as

$$T_f = \sum_i (T_{fi} + 0.5\Delta t\omega_i S_f) \,. \tag{22}$$

For the solid phase, the LBE, EDF, thermal conductivity, and temperature of the solid phase are formulated as

$$T_{si}(\boldsymbol{x} + c\boldsymbol{e}_i\Delta t, t + \Delta t) - T_{si}(\boldsymbol{x}, t)$$
$$= -\frac{1}{\tau''}[T_{si}(\boldsymbol{x}, t) - T_i^{\rm eq}(\boldsymbol{x}, t)] + \Delta t\Big(1 - \frac{1}{2\tau''}\Big)\omega_i S_s \,, \tag{23}$$

$$T_{si}^{\rm eq} = \omega_i\cdot T \,, \tag{24}$$

$$\alpha_{s\varepsilon} = \sigma c_s^2\Delta t(\tau'' - 0.5) \,, \tag{25}$$

$$T_s = \sum_i (T_{si} + 0.5\Delta t\omega_i S_s) \,. \tag{26}$$

We use non-equilibrium extrapolation[31] for boundary conditions of the velocity and temperature fields listed below.

Inlet: $T_s = T_{\rm solar}$, $T_f = T_{\rm amb}$, $u_x = 0.006\ 25$ m/s, $u_y = 0.0$.

Outlet: $\partial T_s/\partial x = 0.0$, $\partial T_f/\partial x = 0.0$, $u_x = u_{\rm out}$, $u_y = 0.0$.

Porous media wall: $\partial T_s/\partial x = 0.0$.

Building wall: $\partial T_f/\partial x = 0.0$, $u_x = u_y = 0.0$, where $T_{\rm solar}$ is the solar radiation temperature obtained from solar radiation $E_{\rm rad} = \kappa\cdot T^4$ (where $E_{\rm rad}$ is the solar radiation incident on the collector), $T_{\rm amb}$ is the ambient temperature, and $u_{\rm out}$ is the sucking velocity of the fan. Taking the velocity field as an example, assuming that the velocity on the boundary node $\boldsymbol{x}_b$ is known, the velocity distribution function can be calculated by

$$f_i(\boldsymbol{x}_b) - f_i^{\rm eq}(\boldsymbol{x}_b) = f_i(\boldsymbol{x}_f) - f_i^{\rm eq}(\boldsymbol{x}_f) \,, \tag{27}$$

where $f_i(\boldsymbol{x}_f)$ is the velocity distribution function of the fluid node next to the boundary node, and $f_i^{\rm eq}(\boldsymbol{x}_b)$ is obtained from Eq. (11). In addition, we also assume that (i) The solar radiation energy is completely absorbed by the collector; (ii) There is no energy loss at the building wall; (iii) The porosity of the porous media wall is uniform.

Table 1 Input parameters for the calculation.

Parameter	Value
$E_{\rm rad}$	600–900 W/m^2
$T_{\rm amb}$	20°C
h_ν	20000 W/(m^3·K)
ν_ϵ	10^{-5}m^2/s
α_f	1.9×10^{-5} m^2/s
C_p	1005 J/(kg·K)
κ	5.67×10^{-8} K^4·m^2/W
$u_{\rm in}$	0.0625 m/s
$u_{\rm out}$	0.0625–1.25 m/s
Wall height	1 m
Outlet width	0.1 m
Porous media wall width	0.025 m
Wall width	0.1 m
ϕ	0.2–0.8
Da	10^{-5}
Ra	10^6

The input parameters and values are listed in Table 1. The output parameters are the collector efficiency, heat exchange effectiveness, and air temperature rises, which measure the thermal performance of the UTC. The collector efficiency $h_{\rm CE}$ is defined as the ratio of useful heat delivered by the solar collector to the total solar energy input on the collector surface[32]

$$h_{\rm CE} = \frac{m_{\rm air,out}C_p(T_{\rm air,out} - T_{\rm amb})}{AE_{\rm rad}} \,, \tag{28}$$

where C_p is the specific heat capacity of air at constant pressure, $T_{\rm air,out}$ is the temperature of the outlet air, A is the collector area, and $m_{\rm air,out}$ is the air mass flow rate at the outlet calculated as $m_{\rm air,out} = vF\rho$, with v being the average velocity at the outlet, F the effective cross-sectional area, and ρ the specific volume of air at constant pressure,[33] whereas the heat exchange effectiveness, $\varepsilon_{\rm HEE}$,[32] is calculated from the ratio of the actual air temperature rise as it passes through the absorber plate to the maximum possible temperature rise

$$\varepsilon_{\rm HEE} = \frac{T_{\rm air,out} - T_{\rm amb}}{T_{\rm col} - T_{\rm amb}}, \tag{29}$$

where $T_{\rm col}$ is the average absorber plate temperature.

We first show the velocity and temperature fields in the solar wall system in Fig. 2. In Fig. 2(a), streamlines together with the velocity magnitude contour are shown. It is seen that the streamlines become dense and velocity magnitude is large adjacent to the duct where the heated air sucked into the building, which is consistent with the previous literature.[33] Figure 2(b) shows the temperature distribution in the solar wall system, indicating how the fresh air is heated in porous media part, and then the temperature of the indoor is rising.

The influence of the fan velocity on the thermal performance of the UTC is shown in Fig. 2. The collector efficiency $h_{\rm CE}$ (Fig. 3(a)) increases whereas the heat exchange effectiveness $\epsilon_{\rm HEE}$ (Fig. 3(b)) decreases as the fan velocity increases, which is again in agreement with previous result.[32]

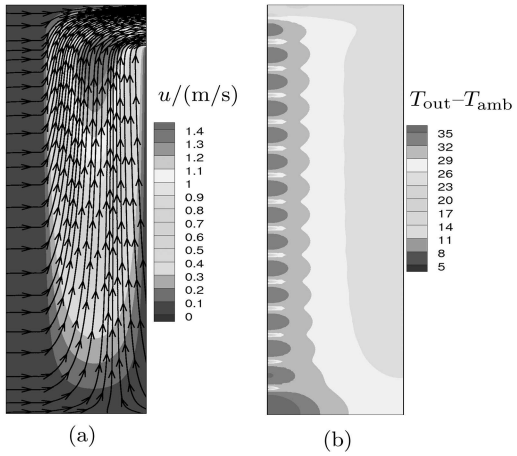

Fig. 2 (Color online) (a) Streamline and velocity field and (b) temperature field of the UTC.

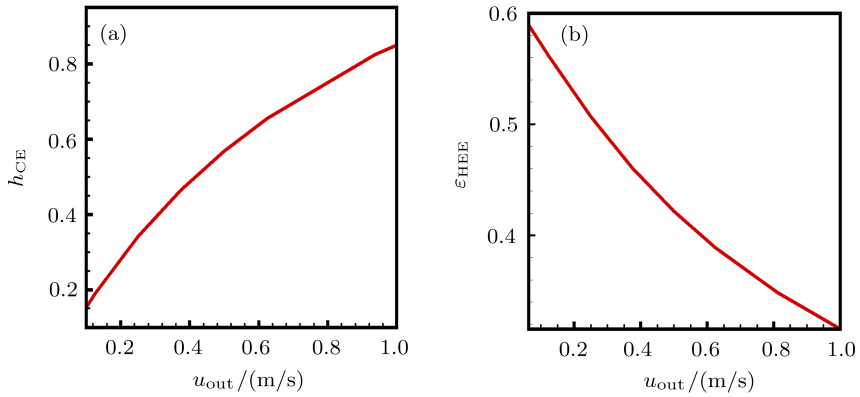

Fig. 3 Effect of fan velocity on (a) the collector efficiency and (b) the heat exchange effectiveness.

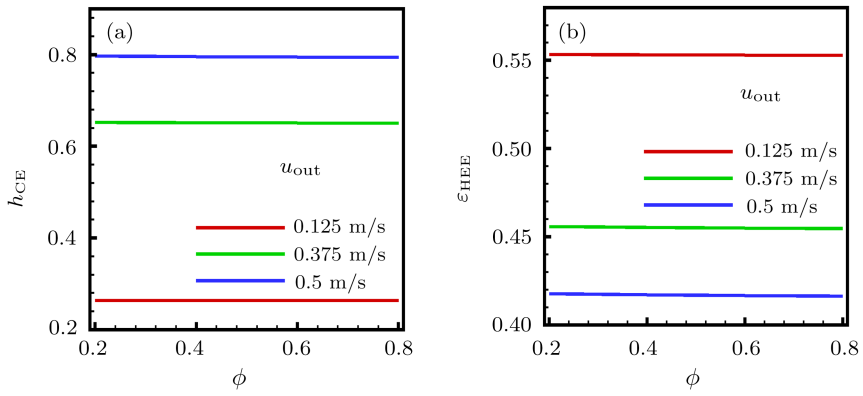

Fig. 4 Effect of porosity on (a) the collector efficiency and (b) the heat exchange effectiveness.

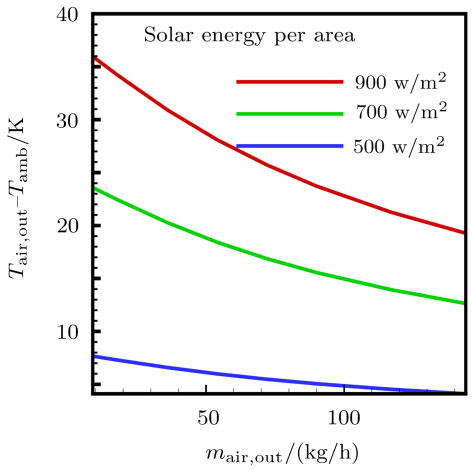

Fig. 5 Effect of radiation intensity and flow rate on air temperature rise.

Figure 4 examines the effect of porosity on the thermal performance at a solar radiation intensity of 900 W/m^2 and three fan velocities. Both the heat exchange effectiveness and collector efficiency decrease marginally when the porosity increases. The collector efficiency drops 0.3 % in Fig. 4(a) and the heat exchange effectiveness drops 0.1 % in Fig. 4(b) as the porosity increases from 0.2 to 0.8, implying that porosity's effect is negligible in the current system setting.

Figure 5 presents the relation between temperature increase and the mass flow rate of the air at three different levels of solar radiation with give ambient temperature of 293 K and porosity of 0.4. The airflow rate is varied from 9 to 150 kg/h. As indicated in the figure, the solar radiation energy change from 900 to 500 W/m^2, corresponding, the exit air temperatures can vary from 29 to 56 in °C.

The proposed LBE model has simulated the fluid dynamics and heat transfer in a UTC with good agreements with published results, demonstrating that LBM is a reliable computational tool for such a complex flow. The results demonstrate that with the current system setting, both fan velocity and solar radiation intensity have significant effect on the thermal performance of the UTC whereas porosity has negligible effect on the heat collector. In actual applications, porous media should play a role to promote the thermal performance of UTCs implying that the current system setting needs to be modified. We are currently conducting simulations of different system setting and surrounding conditions and expect to optimize both factors and provide useful information for the design of next generation of UTCs. The results will be submitted for publication in near future.

References

[1] S. Chen and G.D. Doolen, Ann. Rev. Fluid Mech. **30** (1998) 329.
[2] C.K. Aidun and J.R. Clausen, Ann. Rev. Fluid Mech. **42** (2010) 439.
[3] H. He and L.S. Luo, Phys. Rev. E **56** (1997) 6811.
[4] S. Chen, *et al.*, Phys. Rev. Lett. **67** (1991) 3776.
[5] S. Chen, *et al.*, Comput. Chem. Eng. **19** (1995) 617.
[6] M. Swift, *et al.*, Phys. Rev. E **54** (1996) 041.
[7] A.G. Xu, G. Gonnella, and A. Lamura. Phys. Rev. E **67** (2003) 056105.
[8] A.G. Xu, G. Gonnella, and A. Lamura, Phys. Rev. E **74** (2006) 011505.
[9] Y.B. Gan, A.G. Xu, G.C. Zhang, Y.J. Li, and H. Li, Phys. Rev. E **84** (2011) 046715.
[10] Z.L. Guo and T.S. Zhao, Phys. Rev. E **66** (2002) 036304.
[11] G.H. Tang, W.Q. Tao, and Y.L. He, Phys. Rev. E **72** (2005) 056301.
[12] E.S. Boek, J. Chin, and P.V. Coveney, Int. J. Mod. Phys. B **17** (2003) 99.
[13] http://www.nrel.gov/docs/fy01osti/30176.pdf.
[14] C.J. Wang, W.J. He, and Y.B. Xue, Architectural Journal **3** (2004) 76 (in Chinese).
[15] C.F. Kutscher, C.B. Christensen, and G.M. Barker, J. Sol. Energy Eng. **115** (1993) 182.
[16] C. Dymond and C. Kutscher, *ASME Int. Solar Energy Conf. (Maui)*, ASME Press, New York (1995) p. 1165.
[17] S.J. Arulanandam, K.G.T. Hollands, and E. Brundrett, Sol. Energy **67** (1999) 93.
[18] J.C. Hollick, Renewable Energy **5** (1994) 415.
[19] J.C. Hollick, Renewable Energy **9** (1996) 703.
[20] J.C. Hollick, Renewable Energy **15** (1998) 195.
[21] W. Chen and W. Liu, Acta Energiae Solaris Sinica **26** (2005) 882 (in Chinese).
[22] G.W.E. Van Decker and K.G.T. Hollands, *ISES Solar World Congress (Jerusalem) Vol. 3*, International Solar Energy Society, Freiburg (1999) p. 23.
[23] J.G. Shao, Y. Liu, and Y.S. Xu, Adv. Mater. Res. **322** (2001) 61.
[24] J. Xu, Housing Science **2** (2006) 25.
[25] C.J. Wang, W.J. He, and Y.B. Xue, Architectural Journal **4** (2004) 24 (in Chinese).
[26] C.J. Wang, Y.B. Xue, and Y. Yue, Journal of Shangdong Institute of Architecture and Engineering **18** (2003) 35 (in Chinese).
[27] Z.L. Guo, C.G. Zheng, and B.C. Shi, Phys. Rev. E **65** (2002) 046308.
[28] O.Y. Li and L. Wei, *Proc. Inaugural US-EU-China Thermophysics Conference (Beijing)*, ASME Press, New York (2009) p. 62
[29] M.R. Wang, N. Pan, J.K. Wang, and S.Y. Chen, Commun. Comput. Phys. **2** (2007) 1055.
[30] W.W. Yan, *et al.*, Int. J. Mod. Phys. C **17** (2006) 771.
[31] Z. Guo and T.S. Zhao, Numer. Heat Transfer, Part B **47** (2005) 157.
[32] Augustus Leon M and S. Kumar, Sol. Energy **81** (2007) 62.
[33] C.J. Wang, *et al.*, Proc. Sixth Int. Conf. Enhanced Building Operations (Shenzhen) Energy Systems Laboratory, College Station, TX ESL-IC-06-11-268 (2006).